J Neurophysiol 96: 2972–2983, 2006.
First published August 9, 2006; doi:10.1152/jn.00459.2006.

Network Architecture, Receptive Fields, and Neuromodulation: Computational and Functional Implications of Cholinergic Modulation in Primary Auditory Cortex

Gabriel Soto,[1,2,3] Nancy Kopell,[1,2,3] and Kamal Sen[1,2,4,5]

[1]*Center for BioDynamics,* [2]*Program in Mathematical and Computational Neuroscience,* [3]*Department of Mathematics and Statistics,* [4]*Department of Biomedical Engineering, and* [5]*Hearing Research Center, Boston University. Boston, Massachusetts*

Submitted 1 May 2006; accepted in final form 1 August 2006

Soto, Gabriel, Nancy Kopell, and Kamal Sen. Network architecture, receptive fields, and neuromodulation: computational and functional implications of cholinergic modulation in primary auditory cortex. *J Neurophysiol* 96: 2972–2983, 2006. First published August 9, 2006; doi:10.1152/jn.00459.2006. Two fundamental issues in auditory cortical processing are the relative importance of thalamocortical versus intracortical circuits in shaping response properties in primary auditory cortex (ACx), and how the effects of neuromodulators on these circuits affect dynamic changes in network and receptive field properties that enhance signal processing and adaptive behavior. To investigate these issues, we developed a computational model of layers III and IV (LIII/IV) of AI, constrained by anatomical and physiological data. We focus on how the local and global cortical architecture shape receptive fields (RFs) of cortical cells and on how different well-established cholinergic effects on the cortical network reshape frequency-tuning properties of cells in ACx. We identify key thalamocortical and intracortical circuits that strongly affect tuning curves of model cortical neurons and are also sensitive to cholinergic modulation. We then study how differential cholinergic modulation of network parameters change the tuning properties of our model cells and propose two different mechanisms: one intracortical (involving muscarinic receptors) and one thalamocortical (involving nicotinic receptors), which may be involved in rapid plasticity in ACx, as recently reported in a study by Fritz and coworkers.

INTRODUCTION

Classically, the receptive field (RF) is typically thought of as a description of a single neuron (Dayan and Abbott 2001). However, the response properties of a neuron can be dramatically shaped by the properties of the network in which it is embedded (Destexhe and Marder 2004; Kenet et al. 2003; Tsodyks et al. 1999). This observation suggests a link between cortical network architecture and the cortical RF. Although this relationship has been explored in visual cortex (Miller 2003), the nature of this relationship is poorly understood in primary auditory cortex (ACx).

Cortical networks can be modulated "on-line" by a variety of neuromodulators. Specifically, acetylcholine (ACh) is thought to play an important role in regulating cortical networks during attention and performance of behavioral tasks (Hasselmo and McGaughy 2004). A particularly important function of ACh may be to modulate the relative importance of thalamocortical versus intracortical processing, through the suppression of recurrent excitation (Gil et al. 1997; Hasselmo 1995; Kimura 2000) and enhancement of thalamocortical transmission (Clarke 2004). ACh is also one of the major modulators of auditory cortical activity (Edeline 2003) and similar cholinergic effects have been observed in ACx (Hsieh et al. 2000). Yet, how these cholinergic actions affect auditory cortical RFs remains unclear.

Cortical RFs can change dynamically during attentive behavior. Such changes have recently been reported in ACx; after training in a tone-detection task, the *spectro-temporal receptive fields* (STRFs) of neurons in ACx showed changes localized around the target tone frequency during attentive behavior (Fritz et al. 2003). Can cholinergic modulation of auditory cortical network architecture explain such effects? Specifically, which cholinergic mechanisms are consistent with the observed changes? Computational models of ACx can play an important role in clarifying how network architectures shape RF structure, as they have in the visual cortex (reviewed in Miller 2003). Recent experiments in the auditory system, particularly using dual recordings in the thalamus and cortex and the thalamocortical slice preparation, revealed new information about the architecture of the auditory thalamocortical network, which provide critical constraints for computational models of ACx (Cruikshank et al. 2002; Kaur et al. 2004; Miller et al. 2001a,b, 2002).

In this paper, we develop a computational model of layers III/IV, the main thalamo-recipient layer of ACx (Winer 1992), based on anatomical and physiological data, incorporating recent experimental findings. The paper is organized in two parts. In the first part we systematically explore how changing the architecture of the model network, by changing different network parameters, affects the RFs of model neurons. These simulations provide a general understanding of the effects of auditory cortical network architecture on RFs and allow us to identify key network parameters that provide sensitive targets for neuromodulation. In the second part, we simulate specific effects of ACh in our model network and examine resulting changes in RF structure. These simulations provide insights into potential effects of cholinergic modulation on RFs and also allow us to identify candidate cholinergic mechanisms underlying changes in RFs. Our results suggest two different mecha-

Address for reprint requests and other correspondence: K. Sen, Department of Biomedical Engineering, Boston University, 44 Cummington St., Boston, MA 02215 (E-mail: kamalsen@bu.edu).

The costs of publication of this article were defrayed in part by the payment of page charges. The article must therefore be hereby marked "*advertisement*" in accordance with 18 U.S.C. Section 1734 solely to indicate this fact.

nisms that can explain the experimentally observed changes in RF structure observed in Fritz et al. (2003).

METHODS

Local network

We constructed a network model for layers III/IV of ACx, the first stage of cortical processing in the central auditory pathway (see *scheme* in Fig. 1). Following a fundamental principle of auditory cortical organization, the network is tonotopically organized in an array of frequency channels. Cells in a frequency channel respond to a particular sound frequency. We modeled two cell populations within each frequency channel: excitatory regular-spiking pyramidal cells (E) and inhibitory fast-spiking basket cells (I) (Cruikshank et al. 2002) (see Fig. 1); we represent each population by a single E and a single I cell, respectively. Neurons within a given frequency channel were described by a conductance-based model following Kopell et al. (2000). The units of conductance are mS/cm^2; those of currents are μA/cm^2; those of capacitance are μF/cm^2; those of voltage are mV; and those of time are ms. The E cells in our network were modeled after the primary recipients of thalamic inputs in ACx: excitatory regular-spiking pyramidal neurons in layers III/IV, which display spike-frequency adaptation (Connors and Gutnik 1990; Cruikshank et al. 2002; McCormick et al. 1985) (see Fig. 1). The membrane potential for an E cell is given by

$$C\frac{dV_e}{dt} = -I_{leak,e} - I_{K,e} - I_{Na,e} - I_{Ca,e} - I_{AHP,e} - I_{syn} - I_{app,e} \quad (1)$$

where $C = 1$ and $I_L = -1(V_e + 69)$ is the leak current. The voltage-dependent currents are described by Hodgkin–Huxley formalism. Thus each gating variable follows

$$\frac{dx}{dt} = \alpha(V_e)[1 - x(V_e)] - \beta(V_e)x = \frac{x_{\infty,e}(V_e - x)}{\tau_e(V_e)} \quad (2)$$

The sodium current $I_{Na} = 100m_{\infty,e}^3 h_e(V_e - 50)$, where $m_{\infty,e} = \alpha_{m,e}/(\alpha_{m,e} + \beta_{m,e})$, $\alpha_{m,e} = 0.32(50 + V_e)/\{1 - \exp[-(V_e + 50)/4]\}$, $\beta_{m,e} = 0.28(V_e + 27)/\{\exp[(V_e + 27)/5] - 1\}$, $\alpha_{h,e} = 0.128\exp[-(50 + V_e)/18]$, and $\beta_{h,e} = 4/\{1 + \exp[-(V_e + 27)/5]\}$. The delayed rectifier $I_K = 80n_e^4(V_e + 100)$, where $\alpha_{n,e} = 0.032(V_e + 52)/\{1 - \exp[-(V_e + 52)/5]\}$ and $\beta_{n,e} = 0.5\exp[-(57 + V_e)/40]$. The calcium current $I_{Ca} = g_{Ca}m_\infty^2(V_e - 120)$, where $g_{Ca} = 1$ and $m_\infty = 1/\{1 + \exp[-(V_e + 17)/9]\}$. The voltage-independent calcium-activated potassium current $g_{AHP}([Ca]) = g_{AHP}[Ca]/(K_D + [Ca])$, where $K_D = 30/4$ μM. The intracellular calcium concentration is governed by

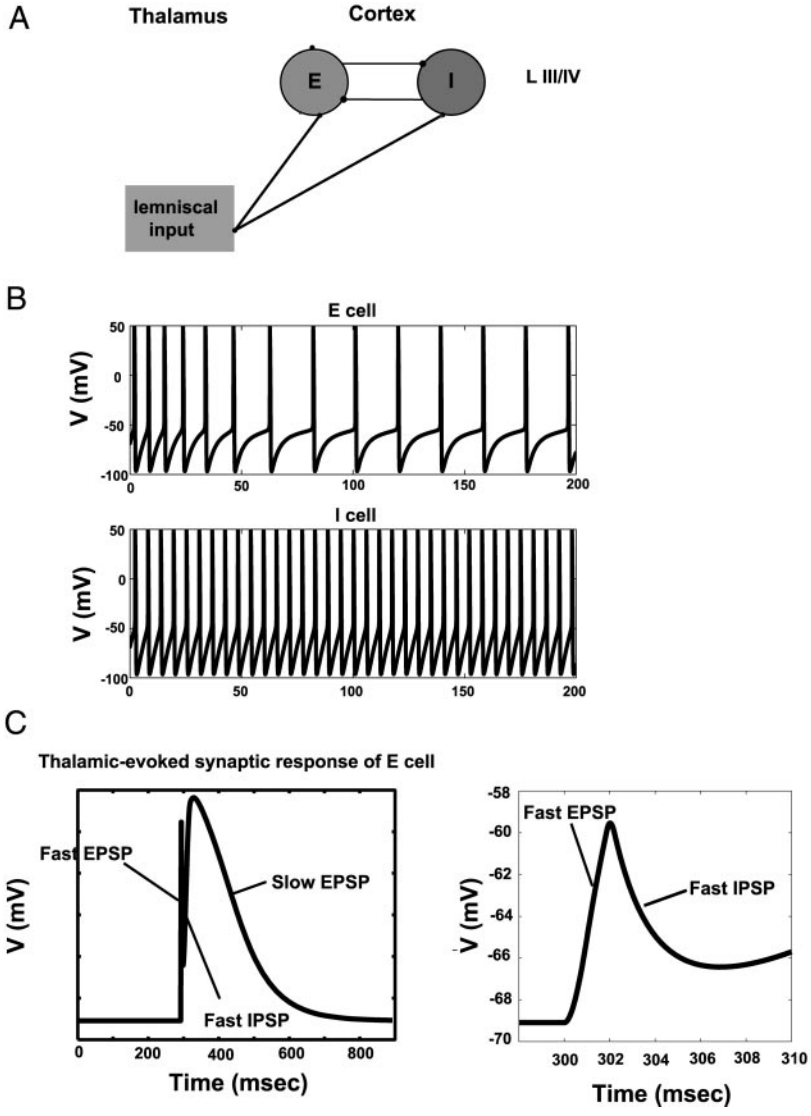

FIG. 1. Responses of model cells to different inputs. *A*: schematic representation of the local network within each frequency channel. *B*: responses of single regular-spiking pyramidal cells (E) and inhibitory fast-spiking basket cells (I) to step depolarizations ($I_{app} = 9$ for E cell, $I_{app} = 7$ for I cell), showing the frequency-adaptation properties of regular-spiking (RS) cells. *C*: response of E cell to single pulse of excitation at thalamocortical synapse. We set $I_{Na} = 0$ in *Eq. 1* in METHODS, to show the profiles of synaptic currents elicited by thalamic stimulation. We chose parameters to generate model responses similar to experimental data, reported in Cruikshank et al. (2002).

$$\frac{d[Ca]}{dt} = -\alpha I_{Ca} - [Ca]/\tau_{Ca}$$

where $\alpha = 0.002\ \mu M(ms\ \mu A)^{-1}cm^2$ and $\tau_{Ca} = 80$ ms. The strength of the afterhyperpolarization (AHP) current was such that, on tonic stimulation, there is a 50% reduction in the firing rate, resulting from frequency adaptation, as shown in different experiments (Cruikshank et al. 2002; Smith and Populin 2001; Wang 1998).

The I cells in our network were modeled after inhibitory fast-spiking interneurons (basket cells), which can fire at higher rates without showing frequency adaptation (Connors and Gutnik 1990; Cruikshank et al. 2002; McCormick et al. 1985); see Fig. 1. The membrane potential for a specific I cell is given by

$$C\frac{dV_i}{dt} = -I_{leak,i} - I_{K,i} - I_{Na,i} - I_{syn} - I_{app,i} \quad (3)$$

where I_L, I_{Na}, and I_K are as before, except that $\alpha_{m,i} = 0.32(44.5 + V_i)/\{1 - \exp[-(V_i + 44.5)/4]\}$. I_{syn} in *Eqs. 1* and *3* represents all synaptic currents that affect a single neuron. We classify synaptic currents as *local intracortical* synaptic currents corresponding to synaptic connections within each frequency channel; *global intracortical* synaptic currents, which represent synaptic connections between cell populations among different frequency channels; and *thalamocortical* synaptic currents that correspond to synaptic connections between relay cells in the thalamus and LIII/IV cortical cells.

LOCAL INTRACORTICAL SYNAPTIC CURRENTS. The I cell inhibits the E cell by γ-aminobutyric acid type A ($GABA_A$)–like synaptic current, represented by $I^l_{syn,e} = g^l_{ie}s^l_{ie}(V_e + 80)$, with $g^l_{ie} = 1$ (the superscript l refers to local synaptic connections within a given frequency channel). The E cell excites the I cell by an α-amino-3-hydroxy-5-methyl-4-isoxazolepropionic acid (AMPA)–like synaptic current represented by $I^l_{syn,i} = g^l_{ei}s^l_{ei}V_i$, with $g^{ei} = 0.5$. The parameter values for g^l_{ie} and g^{ei} are such that tonic stimulation to E cells generates oscillations in the gamma-frequency range (Metherate and Cruikshank 1999; Sukov and Barth 2001). The synaptic variables, corresponding to excitatory and inhibitory synaptic currents are given, respectively, by

$$\frac{ds^l_{ie}}{dt} = [1 + \tanh(V_i/4)](1 - s^l_{ie}) - s^l_{ie}/10 \quad (4)$$

$$\frac{ds^l_{ei}}{dt} = 2[1 + \tanh(V_e/4)](1 - s^l_{ei}) - S^l_{ei}/2 \quad (5)$$

Global network

Frequency channels in our network were arranged in a tonotopic array, a fundamental feature of cortical organization (Read et al. 2002). The network consists of 31 frequency channels, each representing a single auditory frequency, and they are arranged so that six channels equal one octave on the frequency axis.

GLOBAL INTRACORTICAL SYNAPTIC CURRENTS. We assume that different frequency channels are connected by *recurrent excitation* (E-to-E connections), supported by experimental data in Kaur et al. (2004), with a connectivity profile given by

$$g^{Cx}_{ee}(x) = g^{Cx}_{ee}\exp\left[\frac{-(x - x_0)^2}{4(\sigma^{Cv}_{ee})^2}\right] \quad (6)$$

where $g^{Cx}_{ee}(x)$ represents the strength of the synaptic conductance between channel x and the channel x_0, where $x_0 = 1, \ldots, 31$. In all our simulations, we assume $\sigma^{Cx}_{ee} = 8$ so that intracortical recurrent excitation is broad (Kaur et al. 2004); g^{Cx}_{ee} is taken to be a parameter. We include other types of global connectivities: E to I, I to E, and I to I with parameters $g^{Cx}_{ei}(x)$, σ^{Cx}_{ei}, $g^{Cx}_{ie}(x)$, σ^{Cx}_{ie}, $g^{Cx}_{ii}(x)$, and σ^{Cx}_{ii}, respectively. The connectivity profile of such architectures is given in a similar fashion by *Eq. 6*. For simplicity, we assume that all connectivity footprints were Gaussian with parameters g^{Cx}_* and σ^{Cx}_*, similar to those of recurrent excitation, as defined in *Eq. 6* and, for definiteness $g^{Cx}_* \le g^l_*$ and $s^{Cx}_* \le s^{Cx}_{ee}$. In all different interchannel connectivities, the corresponding synaptic variables are identical and given by *Eqs. 4* and *5*.

THALAMIC SYNAPTIC CURRENTS. A single thalamic input to the cortical layer was modeled as a short pulse of excitation (see Fig. 2). Such an input would correspond to stimulating the ventral part of the medial geniculate body (vMGB), thus activating the lemniscal pathway (Cruikshank et al. 2002). Lemniscal thalamic inputs provide simultaneous excitation to both E and I cell populations within each frequency channel in the cortical layer (Cruikshank et al. 2002). Thus E cells received monosynaptic excitation [feedforward excitation (FFE)] and disynaptic inhibition [feedforward inhibition (FFI)], consistent with experimental observations (Cruikshank et al. 2002; Tan et al. 2004; Wehr and Zador 2003). Moreover, it was also shown that thalamic FFE onto E cells is composed of both AMPA- and *N*-methyl-D-aspartate (NMDA)–like synaptic currents and thalamic FFI onto E cells consists of $GABA_A$-like currents, within each frequency channel (see Fig. 1). We model the synaptic currents elicited by thalamic stimulation as

$$I^{Th}_{syn,j} = g^{Th}_j(x)B^{Th}_j S^{Th}_j(V_j - E_{syn}) \quad j = i, e \quad (7)$$

where $g^{Th}_j(x)$ is the maximal synaptic conductance of cell type j (see *Eq. 9* below). B^{Th}_j is either 1, in the case of AMPA/kainate and GABA synaptic currents, or $B^{Th}_j = 1/\{1 + \exp(-0.02V_e)[Mg]/3.57\}$ corresponding to the voltage dependency exhibited by NMDA receptors adapted from Destexhe and Sejnowski (2001); here [Mg] = 1 mM. s^{Th}_j is the synaptic gating variable. At thalamocortical synapses, $E_{syn} = 0$ corresponds to the reversal potentials for AMPA/kainate and NMDA. The dynamics of the thalamocortical synaptic gating variables are given by

$$\frac{ds^{Th}_j}{dt} = \alpha^{Th}_j C^{Th}(1 - s^{Th}_j) - \beta^{Th}_j s^{Th}_j \quad j = i, e \quad (8)$$

where α^{Th}_j and β^{Th}_j are the activation and inactivation rate constants and C^{Th} is the concentration of glutamate released by thalamocortical cells. We assume instantaneous release and uptake of glutamate; i.e., C^{Th} is different from zero for 1 ms; throughout this work $C^{Th} = 0.81$

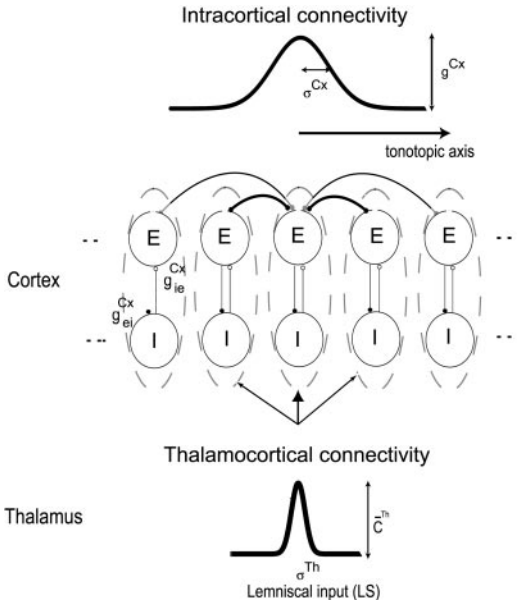

FIG. 2. Schematic of our *canonical* model network, with parameters described in METHODS.

mM. Rate constants for thalamic AMPA: $\alpha_e^{Th} = 1$, $\alpha_i^{Th} = 20\ \text{mM}^{-1} \cdot \text{ms}^{-1}$), $\beta_e^{Th} = \beta_i^{Th} = 0.33\ \text{ms}^{-1}$; for thalamic NMDA: $\alpha_e^{Th} = 0.5\ \text{mM}^{-1} \cdot \text{ms}^{-1}$, $\beta_e^{Th} = 0.0125\ \text{ms}^{-1}$.

Miller et al. (2001a) showed that this *thalamocortical spread* is focal with a radius of at most 1/3 of an octave. We represent the thalamocortical spread, relative to a position x_0, by defining the maximal conductances, $g_j^{Th}(x)$ in *Eq. 7*, as

$$g_j^{\text{Th}}(x) = g_j^{\text{Th}} \exp\left[\frac{-(x - x_0)^2}{2(\sigma^{\text{Th}})^2}\right] \quad (9)$$

Here, maximal conductances onto E and I cells are $g_e^{Th} = 0.085$ and $g_i^{Th} = 0.25$. For thalamic NMDA currents $g_{e,\text{NMDA}}^{Th} = 0.25$. For all simulations presented in this paper, $\sigma^{Th} = 2$. The maximal conductance of the thalamocortical NMDA current was chosen so that on one thalamic pulse of excitation, E cells elicit at least one action potential; i.e., for $g_{e,\text{NMDA}}^{Th} \geq 0.25$ we get suprathreshold responses even in the presence of FFI. On a single thalamic stimulus, the maximum strength of the thalamocortical synapse onto the I cell within the values of $0.05 \leq g_i^{Th} \leq 0.4$ give rise to a single action potential on the I cells, which sends a single FFI inhibitory postsynaptic current (IPSC) onto the E cells, as in Cruikshank et al. (2002).

In this study, we investigate how our model network responds to focal thalamocortical stimuli. In vivo experiments in which simple tones are presented to the animal suggest that thalamocortical responses are brief and onsetlike responses (Bakin and Weinberger 1991). Because it has been found that thalamocortical neurons can fire ≤80 Hz (fourfold higher than their cortical counterparts; see Miller et al. 2001a), we chose such a stimulus as a possible representative of thalamocortical responses to simple tones. Moreover, we found that the shape of the tuning curves for our model cells is invariant with respect to the frequency of the input (data not shown). Because the work by Fritz et al. (2003) did not measure thalamic responses during training sessions, it is difficult for us to directly relate our thalamocortical stimulation with how the thalamus is relaying information to the cortex during training sessions. However, it is a very interesting issue that we want to investigate further in future work.

Stochastic simulations and data analysis

Each cell in our network receives stochastic inputs by $I_{\text{app,e}}$ and $I_{\text{app,i}}$ in *Eqs. 1* and *3*, so that the spontaneous firing rate of the E cells is of order 1 Hz. We model such spontaneous firing rate by defining $I_{\text{app},*}$ in *Eqs. 1* and *3*, where ε is a normally distributed random variable with mean 0 and SD 1, and we update the value of $I_{\text{app},*}$ every 1 ms. Unless otherwise specified, we stimulate our cortical network at 50 Hz for 100 ms at channel number 16.

We compute the network tuning curves by calculating the average firing rate of each E cell in our network in a time window of 150 ms (we ran 20 simulations for each set of parameters). To quantify our data, we compute Gaussian fits to the resulting tuning curves, with parameters

$$F = a_f \exp\left[-\left(\frac{x - m_f}{2\sigma_f}\right)^2\right] + d_f \quad (10)$$

with a_f, m_f, σ_f, and d_f the parameters we use to fit our data. We performed the data-fitting using nonlinear least-square methods (we used the *lsqcurvefit* function in MATLAB). All simulations were performed in MATLAB, using the default implicit solver *ode15s*.

RESULTS

Basic features of our model network

Figure 1 shows how a single frequency channel in our network responds to different inputs. Figure 1*A* shows a schematic description of the local network, in which both E and I cell populations are reciprocally connected and receive stimulation from frequency-specific thalamic inputs. Figure 1*B* shows the response of our model neurons to step depolarizations: E cells show strong frequency adaptation, arising from the afterhyperpolarization (AHP) current (see METHODS) and I cells in our network do not show frequency adaptation. Figure 1*C* shows the response of E cells to frequency-specific thalamic stimulation. Because frequency-thalamic inputs elicit responses in both E and I cells, E cells effectively receive both feedforward excitation and feedforward inhibition. The parameters in our network were chosen so that they qualitatively resemble experimental data in Cruikshank et al. (2002).

Figure 2 shows a schematic description of our canonical network, in which different frequency channels as described in Fig. 1 are connected by broad E-to-E connections, as experimentally shown in Kaur et al. (2004). The connectivity footprint for E-to-E connections is given by *Eq. 6*, with parameters g_{ee}^{Cx} and σ_{ee}^{Cx}. Frequency-specific thalamic inputs are pulses of excitation at different rates with a narrow Gaussian profile (see METHODS), based on data from Miller et al. (2001a).

Cortical architecture and tuning curves: effects of interchannel E-to-E connections on tuning curves

Figure 3 shows how recurrent excitation (interchannel E-to-E connections) shape the tuning curves of E cells in our canonical network, described in Fig. 2. Figure 3*A* shows the network tuning curves and their corresponding Gaussian fits for different values of g_{ee}^{Cx}. These tuning curves represent the response of each E cell in our network to a single tone-frequency. These curves are also equivalent to single-cell tuning curves, which give the response of a single cell to different tone frequencies along the tonotopic axis. Figure 3*B* shows single-trial raster plots for the corresponding g_{ee}^{Cx} values. Figure 3*C* shows a functional relationship between σ_f^{ee} of our Gaussian fits and g_{ee}^{Cx}. E cells remain strongly tuned (i.e., $\sigma_f^{ee} \simeq 1$) for $0 \leq g_{ee}^{Cx} \leq 0.06$. Then σ_f^{ee} increases and saturates around $\sigma_f^{ee} \simeq 5$ (Fig. 3, *bottom*). In particular, $\sigma_f^{ee} < \sigma_{ee}^{Cx}$ (for our canonical network $\sigma_{ee}^{Cx} = 8$) for the chosen values of g_{ee}^{Cx}. This reduction in σ_f^{ee} relative to σ_{ee}^{Cx} is a consequence of our definition of thalamic spread (see METHODS). A pulse of excitation at a given channel elicits suprathreshold responses on E cells located at most two units away from the input channel. Because of the intrinsic properties of I cells, a pulse of excitation elicits suprathreshold responses on I cells at most five units away from the input channel. Thus responses of E cells located at most four to five units away from the input channel are delayed by thalamic FFI. If we change the strength of the thalamic connection so that only I cells within two units away from input channel show suprathreshold responses, we arrive at $\sigma_f \simeq \sigma^{Th}$ (data not shown).

Simulations of our canonical network suggest that localized thalamic inputs can propagate across the model network in some parameter regimes (Fig. 3*B*). Adding interchannel I-to-E connections (direct inhibition) is a potential way to control such propagating activity. To explore this we simulated I-to-E connections in our network. We assumed the connectivity footprint for direct inhibition to be Gaussian, with parameters g_{ie}^{Cx} and σ_{ie}^{Cx} (see METHODS). Figure 3*D* shows regions in the g_{ee}^{Cx}–g_{ie}^{Cx} parameter space, where we observed propagating activity in our network (we obtained similar bifurcation diagrams for E-to-I connections; data not shown). The spread of

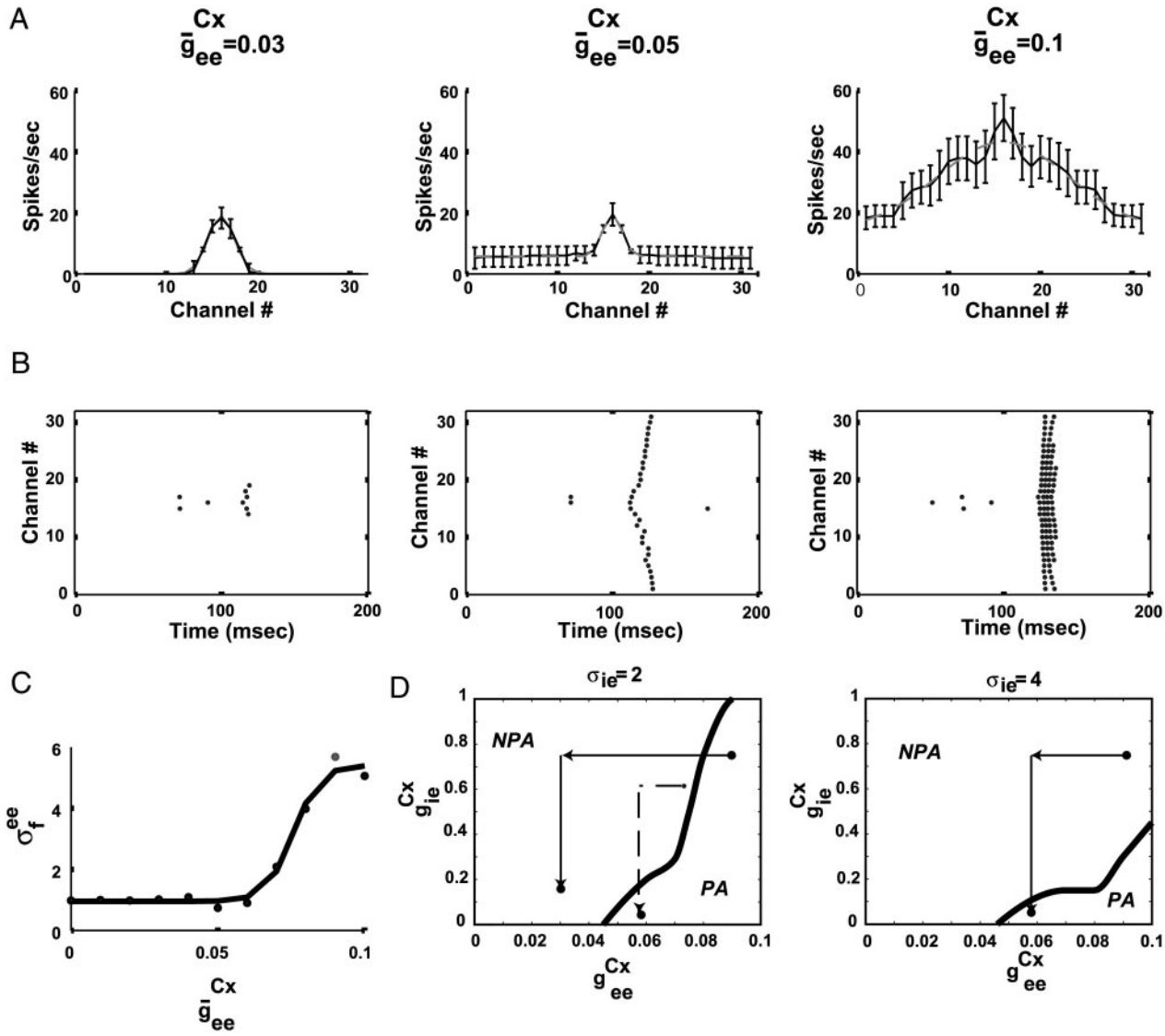

FIG. 3. Simulations of responses of our canonical network to thalamic inputs. $\sigma_{ee}^{Cx} = 8$ and we vary $0 \leq g_{ee}^{Cx} \leq 0.1$. *A*: average firing rates for each E cell across frequency channels (solid lines; error bars show the corresponding SD) and the corresponding Gaussian fit (dashed line) for different values of g_{ee}^{Cx}. For high intracortical (*A*, $g_{ee}^{Cx} = 1$), there are 2 lower peaks around the main peak, centered at the preferred critical frequency (BF). This is explained by the effect of feedforward inhibition, elicited by thalamic stimulation. When intracortical E-to-E connections are strong enough, all cells in our network generate repeated responses (see *B*), i.e., all cells are vigorously excited. However, E cells within the thalamocortical radius [which is around 1/3 of an octave (Miller et al. 2001b)], are also receiving feedforward inhibition, thereby reducing the response of nearby E cells to the BF. *B*: raster plots for single trials for each value of g_{ee}^{Cx}. *C*: relation between g_{ee}^{Cx} and σ_f^{ee}: width of the tuning curve. Resulting sigmoidal function is $2.2280 \tanh[(x - 0.0757)/0.009] + 1.1$. *D*: g_{ee}^{Cx} and g_{ie}^{Cx} parameter region in which thalamocortical stimuli elicits propagating activity (PA) in our model network, i.e., when focal stimulation induces suprathreshold responses in all E cells in our network. NPA, nonpropagating activity. *Left*: region for a spread of intracortical I-to-E connections value of 2 (σ_{ie}^{Cx}; see METHODS). *Right*: region for a spread of intracortical I-to-E connections value of 4 ($\sigma_{ie}^{Cx} = 4$). Both solid and dashed arrows indicate examples of how modulation of both g_{ee}^{Cx} and g_{ie}^{Cx} can modify network propagating activity. We consider a thalamocortical stimulus of 50 Hz for 100 ms.

the intracortical I-to-E connections is a critical factor in determining the size of the region in parameter space in which localized thalamocortical stimuli can spread throughout the network. As σ_{ie}^{Cx} increases, the region for propagating activity decreases (see DISCUSSION for cholinergic effects on propagating activity).

Cholinergic modulation of the cortical network and tuning curves

After exploring how changes in different connectivity parameters affect the tuning properties of cortical cells, we next studied how well-established cholinergic effects on the cortical network affect tuning properties of cortical cells. We divide the results into two categories: muscarinic and nicotinic effects. Within each category, we subdivide these effects into synaptic and intrinsic.

SYNAPTIC MUSCARINIC EFFECTS ON TUNING CURVES. We consider two different muscarinic synaptic effects: suppression of E-to-E connections (Gil et al. 1997; Hasselmo 1995; Hsieh et al. 2000; Kimura 2000) and I-to-E connections (Patil and Hasselmo 1999). Figure 4 shows how such muscarinic synaptic modulation affects the tuning curves of our network E cells. Reduction of recurrent excitation in our canonical network (i.e., reducing g_{ee}^{Cx} from 0.1 to 0.03 in *Eq. 6*) led to sharpening

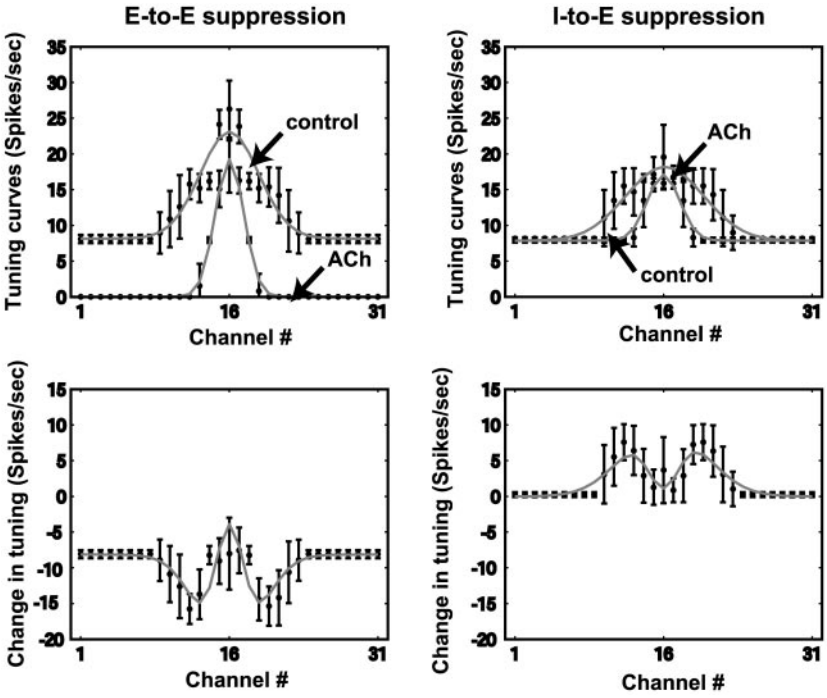

FIG. 4. Synaptic muscarinic modulation of our cortical network. *Left panels*: suppression of E-to-E connections. *Right panels*: suppression of I-to-E synaptic connections. *Top panels*: mean average rates and their corresponding Gaussian fits in control and under cholinergic modulation conditions. *Bottom panels*: difference of mean firing rates and the difference of their corresponding Gaussian fits (solid lines) between the cholinergic case and the control case. *Left panels* (canonical network): $g_{ee}^{Cx} = 0.0.071$ (control), $g_{ee}^{Cx} = 0.03$ [acetylcholinesterase (ACh)], and $\sigma_{ee}^{Cx} = 8$. *Right panels* (canonical network plus I-to-E interchannel connectivity): $g_{ee}^{Cx} = 0.1$, $\sigma_{ee}^{Cx} = 8$, $\sigma_{ie}^{Cx} = 4$, and $g_{ie}^{Cx} = 0.5$ (control case); $g_{ie}^{Cx} = 0.25$ (ACh). When the reduction in g_{ee}^{Cx} is such that strength of the recurrent excitation is less than $g_{ee,crit}^{Cx} \simeq 0.046$, the tuning curves are localized around the BF, for $0 \leq g_{ie}^{Cx} \leq 1$, i.e., the net effect is similar to that shown in the *left panels*. If the reduction of g_{ee}^{Cx} is such that $g_{ee}^{Cx} \geq 0.05$, reduction in g_{ie}^{Cx} would lead to broadening of the tuning curves, similar to the effect shown in *right panels* (not shown).

of tuning curves (Fig. 4, *left panels*). The *top left panel* shows the mean firing rates (solid lines) and their Gaussian fits (dashed lines) in the control case ($g_{ee}^{Cx} = 0.1$) and the ACh case ($g_{ee}^{Cx} = 0.03$). The *bottom left panel* shows the difference between mean firing rates (solid lines) and the difference between Gaussian fits (dashed lines) between the ACh case and the control case. This sharpening was also observed in the different network architectures considered here (data not shown). Suppression of I-to-E connections (i.e., reducing g_{ie}^{Cx} from 0.5 to 0.25 in *Eq. 6*) led to broadening of tuning curves (Fig. 4, *right panels*). The *top right panel* shows the mean firing rates and their Gaussian fits (solid lines) in the control case ($g_{ie}^{Cx} = 0.5$) and the ACh case ($g_{ie}^{Cx} = 0.25$). The *bottom right panel* shows the difference between mean firing rates and the difference between Gaussian fits (solid lines) between the ACh case and the control case.

INTRINSIC MUSCARINIC EFFECTS ON TUNING CURVES. Figure 5 shows the effect of reducing the strength of the AHP current on the tuning curves for different network architectures. We show

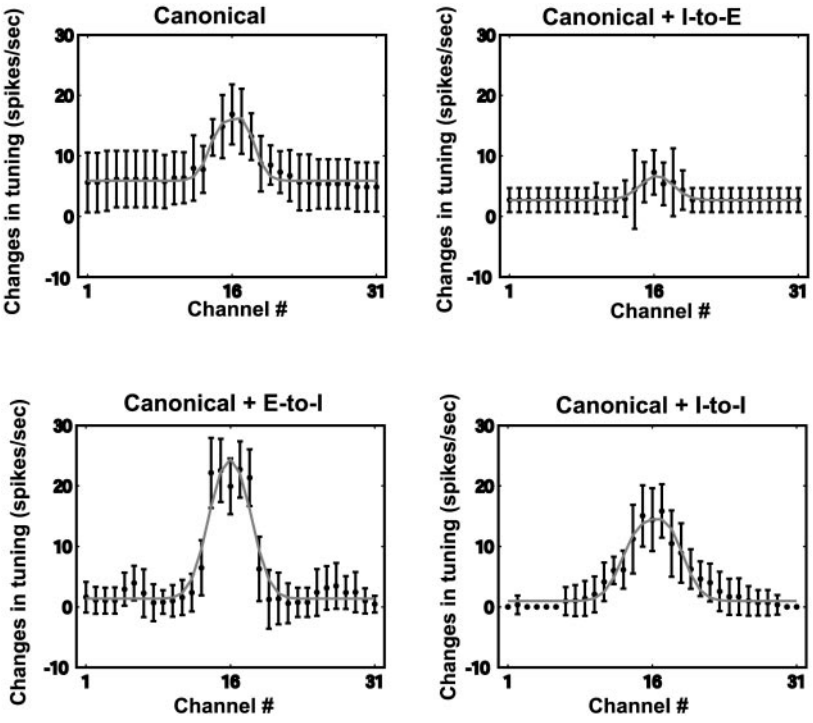

FIG. 5. Intrinsic muscarinic effect [reduction of afterhyperpolarizing (AHP) current] on the tuning properties of the cortical network for different architectures. We show the difference of mean firing rates (solid lines) between the control case and the cholinergic effect (we also show the difference between the corresponding Gaussian fits, dashed lines). *Top left*: $g_{ee}^{Cx} = 0.05$, $\sigma_{ee}^{Cx} = 8$. *Top right*: $g_{ee}^{Cx} = 0.1$, $\sigma_{ee}^{Cx} = 8$, $g_{ie}^{Cx} = 0.5$, $\sigma_{ie}^{Cx} = 2$. *Bottom left*: $g_{ee}^{Cx} = 0.1$, $\sigma_{ee}^{Cx} = 8$, $g_{ie}^{Cx} = 0.25$, $\sigma_{ie}^{Cx} = 8$. *Bottom right*: $g_{ee}^{Cx} = 0.03$, $\sigma_{ee}^{Cx} = 8$, $g_{ii}^{Cx} = 0.5$, $\sigma_{ii}^{Cx} = 8$. In all cases, $K_D = 30$ for the reduced AHP current (see METHODS).

the difference in mean firing rates and the difference between their Gaussian fits (solid lines) between the ACh case ($K_D = 30$ μM) and the control case ($K_D = 7.5$ μM). The net effect was a global increase in the firing rate (i.e., increase in a_f^*) without changing the spread of the tuning curve (i.e., without significant changes in σ_f^*).

SYNAPTIC NICOTINIC EFFECTS ON TUNING CURVES. Here, we show how activation of nicotinic receptors at thalamocortical synapses affects the tuning properties of the cortical network. This nicotinic effect is presynaptic and results in an increase in the amount of glutamate released at the thalamocortical synapse (Clarke 2004). We simulate this effect by doubling C^{Th} in *Eq. 9*. Figure 6 shows the difference in mean firing rates and their corresponding Gaussian fits (solid lines) between the ACh case ($C^{Th} = 1.62$) and the control case ($C^{Th} = 0.81$). The general effect of activation of nicotinic receptors is an increase in the firing rate, but only close to the input channel (no. 16), unlike the previous case.

DISCUSSION

Network architecture can be dramatically sculpted by neuromodulators (Edeline 2003), potentially affecting the functional properties of single neurons within the network. The exploration of this fundamental link in small biological networks has revealed important principles in neuroscience (Destexhe and Marder 2004). An understanding of these issues in cortical networks is likely to provide key insights into cortical computations, specifically in the context of transient (Fritz et al. 2003) and long-term plasticity (Weinberger 2004) in awake-behaving animals. Yet, these ideas have rarely been extended to cortical networks, in part because of their daunting complexity.

The relationship between network architecture and single-neuron response properties was explored in visual cortex (reviewed in Miller 2003). However, to the authors' knowledge, such systematic studies of relationships between RF structure and network architecture in auditory cortex are still lacking. Specific effects of neuromodulators such as ACh have been identified experimentally (Gil et al. 1997; Hasselmo 1995; Hasselmo et al. 1997; Hsieh et al. 2000; Kimura 2000). These effects can be simulated in computational models to understand potential effects of neuromodulation on cortical networks, as well as to identify possible mechanisms that can explain observed single-neuron response properties. In this paper, we adopted the computational approach outlined above to investigate the cholinergic modulation of RFs in primary auditory cortex.

In this paper, we developed a computational model of LIII/IV in ACx. We chose these layers because they receive the main lemniscal input from the thalamus and provide input to successive layers in ACx, playing a critical role transmitting and transforming thalamic inputs (Winer 1992). It is important to note that there are some significant differences in the thalamocortical projections in the auditory system compared with the visual/somatosensory system. In the visual and somatosensory cortices, the specific thalamic targets are stellate cells in LIV. However, in the auditory cortex the middle layers are largely devoid of stellate cells and the principal targets are pyramidal neurons in layers III and IV (Huang and Winer 2000; Linden and Schreiner 2003; Smith and Populin 2001; Winer 1992). A variety of recent experimental data were used to constrain our model (see METHODS).

Network architecture and the RF

We studied how the architecture of our canonical network (see Fig. 2) shapes the tuning curves of cortical cells. We found that there is a sigmoidal relationship between the maximal conductance of the interchannel E-to-E synaptic connections in

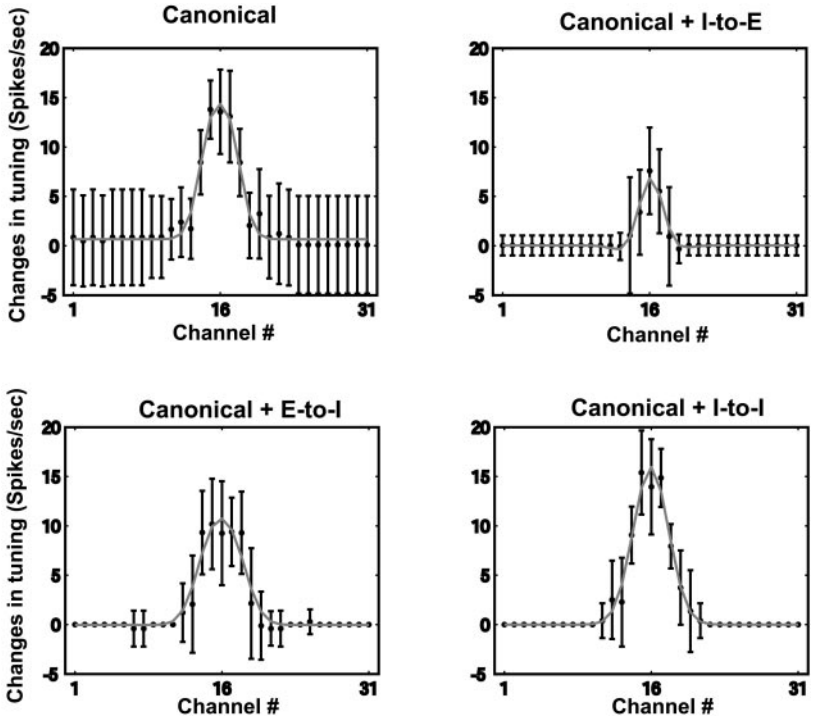

FIG. 6. Nicotinic effect (increase in glutamate release) on the tuning properties of the cortical network for different architectures. We show the difference of mean firing rates (solid lines) between the control case and the cholinergic effect (we also show the difference between the corresponding Gaussian fits, dashed lines). *Top left*: $g_{ee}^{Cx} = 0.05$, $\sigma_{ee}^{Cx} = 8$. *Top right*: $g_{ee}^{Cx} = 0.1$, $\sigma_{ee}^{Cx} = 8$, $g_{ie}^{Cx} = 0.5$, $\sigma_{ie}^{Cx} = 2$. *Bottom left*: $g_{ee}^{Cx} = 0.1$, $\sigma_{ee}^{Cx} = 8$, $g_{ie}^{Cx} = 0.25$, $\sigma_{ie}^{Cx} = 8$. *Bottom right*: $g_{ee}^{Cx} = 0.03$, $\sigma_{ee}^{Cx} = 8$, $g_{ii}^{Cx} = 0.5$, $\sigma_{ii}^{Cx} = 8$. When this nicotinic effect is combined with reduction of recurrent excitation, the resulting changes in tuning curves are similar to the changes shown in this figure, i.e., there is an increase in firing rate around to the BF (data not shown). Similar results are obtained when combined with reduction of I-to-E connections (data not shown).

our canonical network and the width of the tuning curves (Fig. 3, *bottom*). Moreover, the width of the tuning curves was strictly less than the spread of E-to-E cross-channel connectivity; i.e., anatomical and functional network connectivities are not equivalent. This reduction of the functional connectivity relative to the anatomical connectivity is a consequence of the inhibitory circuits within each frequency channel (FFI). The circuitry corresponding to the thalamocortical synapse is such that, on thalamic stimulation, both E and I cells receive the same stimulation; i.e., the anatomical connectivity from the thalamus is the same to E and I cells. However, because of intrinsic and synaptic differences between I (basket) cells and E (pyramidal) cells (see METHODS), I cells are more sensitive to the stimulated thalamic inputs to our model network. As a result, the spread of the suprathreshold responses of I cells to the stimulus is larger than the suprathreshold responses of E cells to the same stimulus. Thus feedforward inhibition, elicited by thalamic stimulation, provides a constraint for how far the information can be relayed by the intracortical circuit. Thus tuning curves obtained from our canonical network are strongly modulated both by feedforward inhibition and recurrent excitation.

One characteristic of our network is that for certain parameter values of interchannel synaptic connections, we observed propagating activity (Fig. 3*D*). Propagating activity has been reported in primary auditory cortex in vitro (Metherate and Cruikshank 1999). To our knowledge, there are no experimental reports of the effects of ACh on propagating activity in auditory cortex, although a recent study in rat prefrontal cortex indicates that ACh can enhance the propagation of "GABA waves" i.e., synchronized activity in inhibitory interneurons in Layer I (Bandyopadhyay et al. 2006), which was not modeled in the present study. We computed bifurcation diagrams with respect to the strength of interchannel E-to-E (g_{ee}^{Cx}) and interchannel I-to-E connections (g_{ie}^{Cx}), to investigate how interchannel connectivity affects propagating activity. We chose these parameters because both are downregulated by ACh (Gil et al. 1997; Hasselmo 1995; Hsieh et al. 2000; Kimura 2000; Patil and Hasselmo 1999). We observed that the larger spread of interchannel I-to-E connections is, the smaller the region over which the network can generate propagating activity (Fig. 3*D*). The effect of ACh on propagating activity depends on the specific trajectory in parameter space imposed by modulation. For instance, in the *left panel* in Fig. 3*D*, if the network is taken from the control condition to the cholinergic modulation condition through the solid lines, then ACh can prevent propagating activity. In contrast, if network follows the dashed lines, ACh can enable propagating activity.

Cholinergic modulation of ACx and potential effects on RFs

A major modulator of ACx is ACh, which originates mainly from nucleus basalis (NB) (Johnston et al. 1979; Lehmann et al. 1980; Mesulam et al. 1983), but also from intrinsic sources within the cortex (Descarries et al. 2004). After exploring the parameter space for our network, we focused on specific cholinergic effects that are known to influence cortical processing. Reduction of AHP or M-currents (Lucas-Meunier et al. 2003) led to a significant increase in the firing rates of E cells in our network for all network connectivities considered (Fig. 5). However, there was no significant change in the spread of the tuning curves (σ_f^*). Thus reduction of AHP currents can lead to a general increase in cortical excitability (a_f) without changes in selectivity (σ_f^*), i.e., frequency selectivity. We found that reduction of recurrent excitation [found in hippocampus (Hasselmo 1995), somatosensory cortex (Gil et al. 1997), visual cortex (Kimura 2000), and auditory cortex (Hsieh et al. 2000)] and weakening of interchannel I-to-E synaptic connections [found in piriform cortex (Patil and Hasselmo 1999)] have opposite outcomes (Fig. 4). Reduction of recurrent excitation sharpens the frequency tuning of cortical cells and may provide higher signal-to-noise ratio and better resolution for sensory processing (Hasselmo and McGaughy 2004). This mechanism renders the cortical network more sensitive to changes at thalamocortical synapses, thereby potentiating the thalamocortical circuit relative to the intracortical one [this effect was recently reported in vivo in primary visual cortex (Roberts et al. 2005)]. On the other hand, reduction of direct inhibition provides a mechanism for broadening frequency tuning of cortical cells, making cortical neurons sensitive to frequencies to which they normally do not respond (see next section). Thus synaptic muscarinic effects provide mechanisms for bidirectional changes in selectivity. Cortical tuning curves can be sharpened or broadened during changes in cortical state, such as from slow-wave sleep to waking (Edeline 2003). Thus the cholinergic effects discussed above may provide mechanisms for state-dependent regulation of RFs. Nicotinic enhancement of the thalamocortical synapse (Clarke 2004) (Fig. 6) led to a significant increase in the firing rate of cortical cells in channels adjacent to the input channel. This provides a thalamocortical mechanism for enhancing the response of cortical neurons near a particular input frequency. In the case of direct inhibition, there is a sharpening of the tuning curves (reduction in σ_f^*), a result of the local circuit at the thalamocortical synapse; i.e., increases in glutamate release at thalamocortical synapses onto inhibitory neurons effectively increases FFI.

Candidate cholinergic mechanisms underlying rapid plasticity in ACx

A recent study by Fritz et al. (2003) demonstrated rapid plasticity of RFs in primary auditory cortex. In their experiments, RFs of cortical neurons were measured in awake behaving ferrets trained to detect a target tone appearing against a background of broadband noise stimuli (TORCS or rippled noise combination). The study found rapid localized changes in RFs around the target tone frequency. Specifically, when a target tone was placed within the receptive field of a cortical neuron (usually at a frequency corresponding to either a neutral or an inhibitory region), the RF at that frequency was transiently enhanced. Such changes in the shape of the RF may arise from the action of neuromodulators, such as acetylcholine on cortical architecture. Simulations of our network suggest two cholinergic mechanisms that could explain experimentally observed changes in RF structure during rapid task-related plasticity in ACx. [Although the following discussion focuses on the experimental paradigm of Fritz et al. (2003), we note that rapid plasticity in RFs has also been induced by classical conditions, e.g., within five trials of conditioning (Edeline et al. 1993).] One of the candidate cholinergic mechanisms is nicotinic enhancement of thalamocortical synapses, which may

underlie facilitative changes in RF structure in the experiments in Fritz et al. (2003). Consider a cortical neuron with a preferred critical frequency (BF) that receives input from a thalamic neuron with a preferred target frequency (TF). If the TF is near the BF of the cortical cell, the tuning curve of the cortical cell would be enhanced at TF (increase in the firing rate; Fig. 6). In this scenario, the spread of thalamocortical connections plays an important role in determining which frequencies in the cortical RF can be enhanced. When the thalamocortical spread is relatively focal, our model predicts that facilitative changes in RFs should also be relatively focal. This is qualitatively consistent with the experimental observations in Fritz et al. (2003). The "local plasticity" effects in the STRF, within 1/3 octave around TF, fits well with the divergence of the functional thalamocortical connectivity, as reported by Miller et al. (2001a), based on dual recordings in thalamus and cortex. An interesting possibility is that recently described "nonfunctional or threshold synapses" that extend beyond 1/3 octave (Lee et al. 2004; Winer et al. 2005) may mediate, under some conditions, "global plasticity" in the STRF, for TFs that are relatively far from BF.

Here we should note that we used the terms "local" and "global" to refer to changes in the RF relatively close to the neurons' BF, whereas in the work of Fritz et al. (2003), "local" plasticity referred to changes in the RF close to the TF. Thus our definition is BF-centric, whereas their definition is TF-centric. Nevertheless, in both cases the important variable is the relative distance between the BF and the TF. Another candidate cholinergic mechanism for observed changes in the RF is the muscarinic suppression of intracortical I-to-E connections, by which cells also become transiently sensitive to target frequencies other than their best frequencies. This disinhibitory effect has been shown to play an important role in changing the signal-to-noise ratio in hippocampus (Haas 1982), neocortex (Kimura and Baughman 1997), and piriform cortex (Patil and Hasselmo 1999). In the Fritz et al. (2003) study, placing the target tone at a frequency corresponding to an inhibitory region in the STRF often abolished or decreased the strength of the inhibitory region. Muscarinic suppression of intracortical I-to-E synapses may explain such a change in RF structure. Depending on the range of intracortical I-to-E connectivity in ACx, this mechanism may not require TF to be close to the BF frequency of the neuron. Interestingly, the most obvious candidate mechanism for facilitative changes in RF structure—strengthening of recurrent E-to-E connections—is not consistent with cholinergic modulation because experimental data suggest that recurrent E-to-E connections are suppressed by ACh (Gil et al. 1997; Hasselmo 1995; Hasselmo et al. 1997; Hsieh et al. 2000; Kimura 2000). However, it remains possible that strengthening of E-to-E connections may be mediated by other neuromodulators (Edeline 2003).

Selective enhancement of receptive fields in vivo

The preceding discussion relates cholinergic effects on RFs in our network model to experimentally observed rapid plasticity in the Fritz et al. (2003) study. However, it raises an important question regarding the selectivity of the observed changes. In the Fritz et al. experiments, the TF is defined by the behavioral task. How can a system translate this behavioral knowledge into selective RF changes at TF—that is, how does the system mark the TF? Although we did not explicitly model the genesis of selectivity, in the next section we provide a biologically plausible explanation of how such selectivity might arise in the system.

CHANGES IN CIRCUITRY DURING TRAINING. In Fritz et al. (2003), ferrets are trained using avoidance conditioning to stop licking water from a spout when they hear a tone, to avoid a mild shock. Training on such a task may lead to a change of connectivity in the system such that, eventually, the tone alone leads to the activation of NB and release of ACh in primary auditory cortex. Such changes in circuitry could occur in the nonlemniscal pathway, involving areas such as the medial part of medial geniculate body (MGm), the posterior intralaminar complex (PIN), the amygdala, and NB (Ji et al. 2005; Weinberger 2004).

CONTEXT (TASK) SPECIFICITY. During training sessions, the target tones are randomized across sequential trials. Because the ferret learns to perform the task with any tone, NB activation and ACh release would be triggered by any tone. Thus although there is no stimulus, i.e., frequency specificity (ACh is released by a tone of any frequency), there is context specificity, i.e., release takes place only when a tone appears during the specific task the animal was trained to perform. In addition to the changes in circuitry during training (see above), top-down influences of attention and expectation may also contribute to the context (task) specificity (Fritz et al. 2005).

STIMULUS (FREQUENCY) SPECIFICITY. During the physiological recording sessions, the STRF of a cortical neuron was mapped in two states: the passive state, when the animal is resting, and the behavioral state, when the animal is performing the task. The difference between the passive STRF and the behavioral STRF is used to quantify rapid plasticity. During the behavioral task, ACh would be released with the target tone in a manner similar to that established by training; i.e., it would be context (task) specific, but not stimulus (frequency) specific. However, a critical difference from the training sessions is that during the behavioral task, the target tone is kept fixed within a given "block" (a sequence of trials). Thus during the period over which the behavioral STRF is measured, a specific target frequency (TF) is repeatedly paired with the release of cortical ACh. This repeated pairing of TF with ACh may induce rapid plasticity in the STRF at TF.

LOCALIZATION/EXTENT OF RAPID PLASTICITY ACROSS FREQUENCIES. As explained earlier, cortical neurons that repeatedly receive both sensory input driven by TF and context-specific ACh would undergo rapid plasticity. Because ACh release is not frequency specific, cortical neurons with a broad range of best frequencies are likely to receive ACh. Thus the specific cortical neurons "marked" for rapid plasticity are those that receive sensory input driven by TF during the task. A sensory input at TF can "spread out" to other frequencies as a result of the divergent connectivity in the system. Thus TF will drive not only a cortical neuron with best frequency TF, but also other cortical neurons with nearby best frequencies. Conversely, limits on the spread of input frequencies would determine the range of cortical neurons driven by TF and thus marked for rapid plasticity. This may explain the localization of the changes in STRFs around TF.

We have discussed above a plausible way to provide frequency specificity in rapid plasticity. However, a potential caveat in this argument is that the dynamics of mechanisms underlying associative plasticity remains poorly understood. What determines the time course of rapid plasticity? Is it determined by the time course of ACh release, the time course for changes in pre- and postsynaptic structures, or both? Is the precision of firing of NB neurons and the time course of the resultant ACh release in cortex sufficient for the required associative plasticity (Kilgard and Merzenich 1998; Weinberger 2003). Such questions are relatively difficult to address at present given the lack of experimental data on the subject (although see Duque et al. 2000; Manns et al. 2000). Future models can incorporate this level of detail, as more experimental constraints become available.

Model predictions and suggested experiments

Our model identified several candidate cholinergic mechanisms underlying rapid plasticity observed in auditory cortical RFs. Although it is plausible that ACh is involved in rapid plasticity, this has not been directly tested. Thus it will be important to first determine the effects of manipulating cortical ACh on rapid RF plasticity, such as by blockade of cholinergic receptors in cortex and/or by lesioning NB. If ACh is implicated in rapid plasticity, further experiments can be aimed at determining the locus of plasticity; i.e., is rapid plasticity mediated by thalamocortical synapses, intracortical synapses, or both? Our model identifies two candidate cholinergic mechanisms—one thalamocortical and one intracortical—that may underlie rapid RF plasticity: modulation of thalamocortical nicotinic receptors and modulation of intracortical muscarinic receptors. Experiments that manipulate nicotinic receptors may be particularly revealing, given that these receptors appear to be localized primarily at thalamocortical synapses (Clarke 2004). Thus blocking nicotinic receptors should abolish, or reduce, rapid plasticity if it is mediated by thalamocortical synapses. On the other hand, if the plasticity is mediated primarily by intracortical synapses, then blocking the nicotinic receptor may not have a substantial effect. In principle, the involvement of muscarinic receptors can also be tested using a similar approach, although the results may be more difficult to interpret because muscarinic receptors are located at both thalamocortical and intracortical synapses.

Future directions

Our computational study investigated cholinergic modulation of RFs, focusing on individual effects of ACh on different parameters, following previous experimental studies (Edeline 2003). Modeling the combined effect of ACh on multiple parameters should await further experimental study, especially because of possible complex interactions between the individual effects. Nevertheless, preliminary simulations of combined effects produced results that were similar to those reported here (see Figs. 4, 5, and 6). Other neuromodulators are also known to affect cortical response properties (Edeline 2003). For instance, noradrenaline (NA) can improve signal-to-noise ratio in sensory cortices (Hasselmo et al. 1997; Manunta and Edeline 2004), by reducing the spontaneous firing rate. NA has also been involved in reducing the strength of E-to-I connections in piriform cortex (Hasselmo et al. 1997). Additional simulations we performed show that reducing the strength of E-to-I synapses has an effect that is similar to reducing direct inhibition (interchannel I-to-E connections), which is accomplished by ACh (data not shown). Thus NA and ACh may both modulate RFs in ACx, using different mechanisms. In particular, this noradrenergic effect could potentially be a third mechanism (intracortical) that could explain the changes in RF structure during tone-detection task experiments in Fritz et al. (2003). Future computational studies should explore the functional effects of noncholinergic modulators, such as NA, serotonin, and dopamine in more detail. Our model focused on layers III/IV because these are the "input layers" in primary auditory cortex and a good starting point for our computational study. The network architecture in other layers is distinct from layers III/IV (Winer 1992). Because neuromodulatory effects occur, in part, through network architecture, it is difficult to extrapolate our results to other layers. Future work extending our model to other cortical layers may reveal a greater diversity of possible changes in RF structures through neuromodulation.

Another class of phenomena not considered in this study is that of dynamic changes in the strength of synapses, such as facilitation and depression. Although these phenomena have been well characterized in the visual and somatosensory cortices (Abbott and Regehr 2004), surprisingly little remains known about these phenomena in auditory cortex. To our knowledge, there is one study in Layer II/III (not modeled in the present study) that has investigated this topic (Atzori et al. 2001). Experimental studies characterizing the temporal dynamics of auditory cortical synapses in other layers and cholinergic effects on temporal dynamics will be particularly valuable in extending the model to include such effects. The work by Fritz et al. (2003) also revealed other types of changes not considered here, notably persistent changes in RF structure that may provide substrates for auditory memories. Long-term plasticity of auditory cortical RFs is a complex topic with a long history that deserves much further computational study (Suga and Ma 2003; Weinberger 2004). We are currently working on extending our computational model to include long-term plasticity of auditory cortical RFs, by including plasticity rules such as spike-timing–dependent plasticity (Soto et al. 2005). Finally, future studies should also explore the interesting task dependency in RF changes revealed in subsequent studies by Fritz et al. (2005), which show that the RF changes induced in a two-tone discrimination task are distinct from those observed in the tone-detection task considered here.

ACKNOWLEDGMENTS

We thank M. Hasselmo for useful comments and remarks on a previous version of this manuscript. We also thank members of Sen Lab and the NaK group for useful inputs and comments.

Present address of G. Soto: Departamento de Matemática, Facultad de Ingeniería, Universidad Nacional de la Patagonia San Juan Bosco, Comodoro Rivadavia, Chubut Argentina.

GRANTS

This work was supported by a Burroughs Wellcome Fund grant to G. Soto and National Institute of Neurological Disorders and Stroke Grant 5R01-NS-46058 and National Science Foundation Grant DMS-0211505 to N. Kopell, and National Institute of Deafness and Other Communication Disorders Grant IROI DC-007610-01A1 to K. Sen.

REFERENCES

Abbott L and Regehr W. Synaptic computation. *Nature* 431: 796–803, 2004.

Atzori M, Lei S, Evans D, Kanold P, Phillips-Tansey E, McIntyre O, and McBain C. Differential synaptic processing separates stationary from transient inputs to the auditory cortex. *Nat Neurosci* 4: 1157–1158, 2001.

Bakin J and Weinberger N. Classical conditioning induces cs-specific receptive field plasticity in the auditory cortex of the guinea pig. *Brain Res* 537: 271–286, 1991.

Bandyopadhyay S, Sutor B, and Hablitz J. Endogenous acetylcholine enhances synchronized interneuron activity in rat neocortex. *J Neurophysiol* 95: 1908–1916, 2006.

Clarke PB. Nicotinic modulation of thalamocortical neurotransmission. *Prog Brain Res* 145: 253–260, 2004.

Connors BW and Gutnik M. Intrinsic firing patterns of diverse neocortical neurons. *Trends Neurosci* 13: 99–104, 1990.

Cruikshank SJ, Rose HJ, and Metherate R. Auditory thalamocortical synaptic transmission in vitro. *J Neurophysiol* 87: 361–384, 2002.

Dayan P and Abbott L. *Theoretical Neuroscience: Computational and Mathematical Modeling of Neural Systems.* Cambridge, MA: MIT Press, 2001.

Descarries L, Mechawar N, Aznavour N, and Watkins K. Structural determinants of the roles of acetylcholine in cerebral cortex. *Prog Brain Res* 145: 45–58, 2004.

Destexhe A and Marder E. Plasticity in single neuron and circuit computations. *Nature* 431: 789–795, 2004.

Destexhe A and Sejnowski T. *Thalamocortical Assemblies: How Ion Channels, Single Neurons and Large-Scale Networks Organize Sleep Oscillations.* Oxford, UK: Oxford Univ. Press, 2001.

Duque A, Balatoni B, Detari L, and Zaborzky L. Eeg correlation of the discharge properties of identified neurons in the basal forebrain. *J Neurophysiol* 84: 1627–1635, 2000.

Edeline J. The thalamo-cortical auditory receptive fields: regulation by the states of vigilance, learning and the neuromodulatory systems. *Exp Brain Res* 153: 554–572, 2003.

Edeline J, Pham P, and Weinberger N. Rapid development of learning-induced receptive field plasticity in the auditory cortex. *Behav Neurosci* 107: 539–551, 1993.

Fritz J, Elhilali M, and Shamma S. Active listening: task-dependent plasticity of spectrotemporal receptive fields in primary auditory cortex. *Hear Res* 206: 159–176, 2005.

Fritz J, Shamma S, Elhilali M, and Klein D. Rapid task-related plasticity of spectrotemporal receptive fields in primary auditory cortex. *Nat Neurosci* 6: 1216–1223, 2003.

Gil Z, Connors B, and Amitai Y. Differential modulation of neocortical synapses by neuromodulators and activity. *Neuron* 19: 679–686, 1997.

Haas HL. Cholinergic disinhibition in hippocampal slices of the rat. *Brain Res* 233: 200–204, 1982.

Hasselmo M. Neuromodulation and cortical function: modeling the physiological basis of behavior. *Behav Brain Res* 67: 1–27, 1995.

Hasselmo M, Linster C, Patil M, Ma D, and Cekic M. Noradrenergic suppression of synaptic transmission may influence cortical signal-to-noise ratio. *J Neurophysiol* 77: 3326–3339, 1997.

Hasselmo M and McGaughy J. High acetylcholine levels set circuit dynamics for attention and encoding and low acetylcholine levels set dynamics for consolidation. *Prog Brain Res* 145: 207–231, 2004.

Hsieh C, Cruikshank S, and Metherate R. Differential modulation of auditory thalamocortical and intracortical synaptic transmission by cholinergic agonist. *Brain Res* 880: 51–64, 2000.

Huang C and Winer J. Auditory thalamocortical projections in the cat: laminar and areal patterns of input. *J Comp Neurol* 427: 302–331, 2000.

Ji W, Ma X, and Suga S. Effects of agonists and antagonists of NMDA and ACh receptors on plasticity of bat auditory system elicited by fear conditioning. *J Neurophysiology* 94: 1199–1211, 2005.

Johnston M, McKinney M, and Coyle J. Evidence for a cholinergic projection to neocortex from neurons in basal forebrain. *Proc Natl Acad Sci USA* 76: 5392–5396, 1979.

Kaur S, Lazar R, and Metherate R. Intracortical pathways determine breadth of subthreshold frequency receptive fields in primary auditory cortex. *J Neurophysiol* 91: 2551–2567, 2004.

Kenet T, Bibitchkov D, Tsodyks M, Grinvald A, and Arieli A. Spontaneously emerging cortical representations of visual attributes. *Nature* 425: 954–956, 2003.

Kilgard M and Merzenich M. Cortical map reorganization enabled by nucleus basalis activity. *Science* 279: 1714–1718, 1998.

Kimura F. Cholinergic modulation of cortical function: a hypothetical role in shifting the dynamics in cortical network. *Neurosci Res* 38: 19–26, 2000.

Kimura F and Baughman RW. Distinct muscarinic receptor subtypes suppress excitatory and inhibitory synaptic response in cortical neurons. *J Neurophysiol* 77: 709–716, 1997.

Kopell N, Ermentrout G, Whittington M, and Traub R. Gamma rhythms and beta rhythms have different synchronization properties. *Proc Natl Acad Sci USA* 97: 1867–1872, 2000.

Lee C, Schreiner C, Imaizumi K, and Winer J. Tonotopic and heterotopic projection systems in physiologically defined auditory cortex. *Neuroscience* 128: 871–887, 2004.

Lehmann J, Nagy J, Atmadia S, and Fibiger H. The nucleus basalis magnocellularis: the origin of a cholinergic projection to the neocortex of the rat. *Neuroscience* 5: 1161–1174, 1980.

Linden J and Schreiner C. Columnar transformations in auditory cortex: a comparison to visual and somatosensory cortex. *Cereb Cortex* 13: 83–89, 2003.

Lucas-Meunier E, Fossier P, Baux G, and Amar M. Cholinergic modulation of the cortical neuronal network. *Eur J Physiol* 446: 17–29, 2003.

Manns I, Alonso A, and Jones B. Discharge properties of juxtacellularly labeled and immunohistochemically identified cholinergic basal forebrain neurons recorded in association with the electroencephalogram in anesthetized rats. *J Neurosci* 20: 1505–1518, 2000.

Manunta Y and Edeline J. Noradrenergic induction of selective plasticity in the frequency tuning of auditory cortex neurons. *J Neurophysiol* 92: 1445–1463, 2004.

McCormick D, Connors B, Lighthall J, and Prince D. Comparative electrophysiology of pyramidal and sparsely spiny stellate neurons of the neocortex. *J Neurophysiol* 54: 782–806, 1985.

Mesulam N, Mufson E, Wainer B, and Levey A. Central cholinergic pathways in the rat: an overview based on an alternative nomenclature (ch1–ch6). *Neuroscience* 10: 1185–1201, 1983.

Metherate R and Cruikshank S. Thalamocortical inputs trigger a propagating envelope of gamma-band activity in auditory cortex in vitro. *Exp Brain Res* 126: 160–174, 1999.

Miller K. Understanding layer 4 of the cortical circuit: a model based on cat v1. *Cereb Cortex* 13: 73–82, 2003.

Miller L, Escabi M, Read H, and Schreiner C. Functional convergence of response properties in the auditory thalamocortical system. *Neuron* 32: 151–160, 2001a.

Miller L, Escabi M, Read H, and Schreiner C. Spectrotemporal receptive fields in the lemniscal auditory thalamus and cortex. *J Neurophysiol* 87: 516–527, 2002.

Miller L, Escabi M, and Schreiner C. Feature selectivity and interneuronal cooperation in the thalamocortical system. *J Neurosci* 21: 8136–8144, 2001b.

Patil MM and Hasselmo M. Modulation of inhibitory synaptic potentials in piriform cortex. *J Neurophysiol* 81: 2103–2118, 1999.

Read H, Winer J, and Schreiner C. Functional architecture of auditory cortex. *Curr Opin Neurobiol* 12: 433–440, 2002.

Roberts M, Zinke W, Guo K, Robertson R, McDonald J, and Thiele A. Acetycholine dynamically controls spatial integration in marmoset primary visual cortex. *J Neurophysiol* 93: 2062–2072, 2005.

Smith P and Populin L. Fundamental differences between the thalamocortical recipient layers of the cat auditory and visual cortices. *J Comp Neurol* 436: 508–519, 2001.

Soto G, Kopell N, and Sen K. A computational model for long-term plasticity in primary auditory cortex. *Abstract, Society for Neuroscience* 2005.

Suga N and Ma X. Multiparametric corticofugal modulation and plasticity in the auditory system. *Nat Rev Neurosci* 4(10): 783–794, 2003.

Sukov W and Barth D. Cellular mechanisms of thalamically evoked gamma oscillations in auditory cortex. *J Neurophysiol* 85: 1235–1245, 2001.

Tan A, Zhang L, Merzenich M, and Schreiner C. Tone-evoked excitatory and inhibitory synaptic conductances of primary auditory cortex neurons. *J Neurophysiol* 92: 630–643, 2004.

Tsodyks, M, Kenet, T, Grinvald, A, and Arieli, A. Linking spontaneous activity of single cortical neurons and the underlying functional architecture. *Science* 286: 1943–1946, 1999.

Wang X. Calcium coding and adaptive temporal computation in cortical pyramidal neurons. *J Neurophysiol* 79: 1549–1566, 1998.

Wehr M and Zador A. Balanced inhibition underlies tuning and sharpens spike timing in auditory cortex. *Nature* 426: 442–446, 2003.

Weinberger N. The nucleus basalis and memory codes: auditory cortical plasticity and the induction of specific, associative behavioral memory. *Neurobiol Learn Mem* 80: 268–284, 2003.

Weinberger NM. Specific long-term memory traces in primary auditory cortex. *Nat Rev Neurosci* 5: 279–290, 2004.

Winer J. The functional architecture of the medial geniculate body and primary auditory cortex. In: *The Mammalian Auditory Pathway: Neuroanatomy*, edited by Webster DB, Popper AN, and Fay RR. New York: Springer-Verlag, 1992, p. 222–409.

Winer J, Miller L, Lee C, and Schreiner C. Auditory thalamocortical transformation: structure and function. *Trends Neurosci* 28: 255–263, 2005.